

Design optimisation of a side impact beam made out of high strength aluminium alloys using Barlat YLD2000 and GISSMO failure model for the “Extended Hotforming Process”

Julian Marc Schlosser¹, Serkan Mouchtar¹, Wolfgang Rimkus¹, Robert Schneider²

¹ Lightweight Construction Centre, Aalen University, Beethovenstraße 1, 73430 Aalen

² Ulm University of Applied Sciences, Albert-Einstein-Allee 55, 89081 Ulm

1 Introduction

The automotive industry is facing new challenges due to stricter CO₂ emission laws. Thus, to design more environmentally-friendly cars, various lightweight construction strategies need to be considered to meet the growing demand for resource efficiency [1]. In order to minimise weight, the lightweight design strategy "design for lightweight construction" is increasingly becoming important for industry. Especially the "structural optimisation" with its sub-areas: topology-, fibre-, thickness- and parameter-optimisation is designated as a very powerful tool for lightweight applications.

In addition, damage and failure modelling is getting more and more important in order to predict the behaviour of any component by FEM-simulations as accurate as possible. For this purpose, the entire material history (from production right through to the crash of the component) must be taken into account. Whereas for forming processes forming limit curves (FLC's) are sufficient to predict the material behaviour failure models, which describe failure as a function of stress states, need to be applied for detailed crash calculations [2].

In this paper the design process of an AA7075 side impact beam will be presented; starting from structural optimisation through to the calibration of a material and a damage model. The geometry of the side impact beam is determined by topology optimisation. Special attention is given towards the temperature control of the forming process since a "Thermal Direct Joining" procedure (e.g. for CFRP-patches) is aimed to be implemented. The high-strength anisotropic aluminium alloy (AA7075) is characterised after applying the Hotforming process (Hotforming condition). Both, the Barlat YLD2000 material model and the GISSMO failure model are calibrated using the graphical optimisation tool *LS-OPT*.

2 Extended Hotforming

Currently, compared to conventional sheet metal forming processes the "Hotforming Process" [3] offers the possibility to produce parts made of high and ultra-high strength aluminium alloys (7xxx group) in a more complex shape. Based on the standard Hotforming process some modifications are made to be able to generate crash components with local reinforcements via an "integrated thermal direct joining step" (see Figure 1).

The advantage of this "Extended Hotforming Process" is that highly stressed areas of crash relevant components can be reinforced with a local patch made of CFRP or GFRP and thus, the sheet thickness of the base material can be further reduced. Another advantage of the Extended Hotforming Process is the short cycle time due to the combination of the forming and joining process compared to the conventional manufacturing process of fibre reinforced parts.

The extension of the Hotforming Process (Figure 1) incorporates several steps: laser structuring the blank (2) prior solution annealing at $T > 465^{\circ}\text{C}$ (3) to ensure a better adhesion of the patch. A subsequent cooling step of the blank (4) to $150\text{-}180^{\circ}\text{C}$ with a cooling rate greater than 100 K/s to avoid irregular segregation of the supersaturated α -solid solution and thus, to achieve highest strength values and to melt the matrix of the thermoplastic patch. This step is crucial since otherwise the patch would be destroyed at temperatures above 465°C . Further, the patch is positioned (5) on the sheet metal (incl. release agent) and put together into the forming press (6) which is also heated up to $150^{\circ}\text{-}180^{\circ}\text{C}$. This is followed by a forming process step in the warm state. At the same time, the thermal direct joining is takes place just by using the residual heat of the sheet metal. Then the part will be cut (7) by laser or directly in the die. The final step is the heat-treatment (8) to improve the strength and corrosion resistance of the 7xxx Al-alloy.

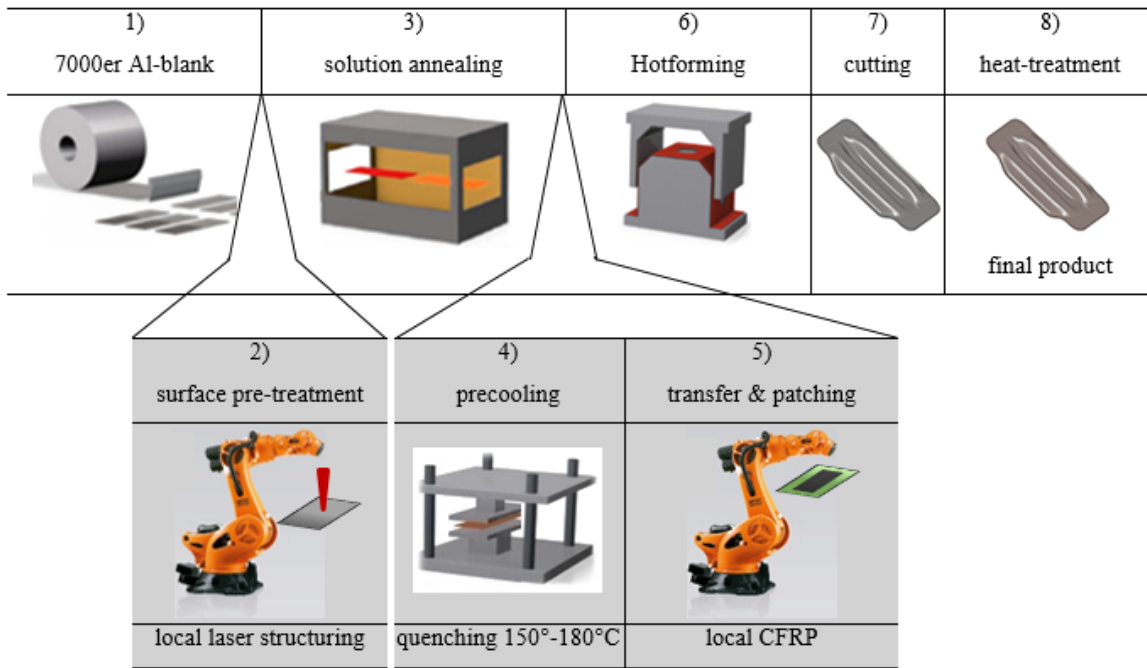


Fig.1: Novel Hotforming Process with integrated thermal direct joining

2.1 Layout test bench

In order to achieve high quality simulation results the material has to be described as accurate as possible. The material behaviour of rolled ultra-high-strength aluminium alloys is getting anisotropic especially if exposed to multi-axial stress conditions. For this reason, anisotropic material models such as Barlat2000 [4] or Barlat89 [5] are used for the forming simulations. In order to be able to characterize the material parameters under realistic conditions an experimental test bench (see Figure 2) was developed and built up. The test bench consists of: a furnace (1), a heated and cooled plate tool integrated into a 20t press (2), a temperature data logger (3), a tensile testing machine with climatic chamber (4) and an optical measuring (GOM Aramis Adjustable – 2.3M) (5). A detailed description of the individual components is given in Table 1.

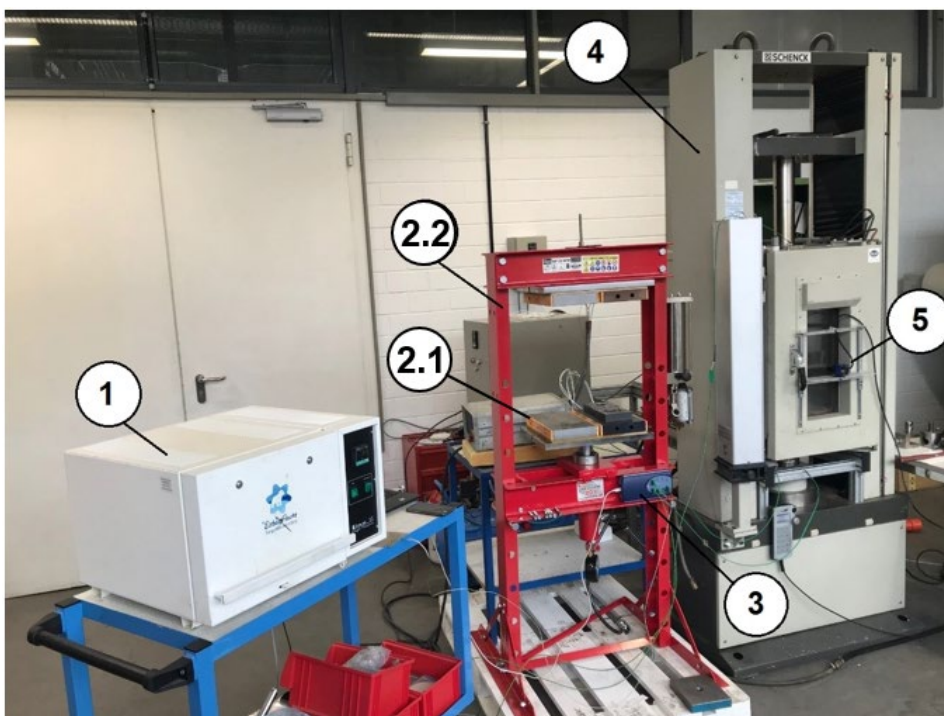


Fig.2: Test bench set-up for forming process at elevated temperature


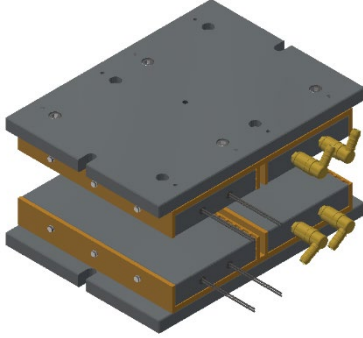
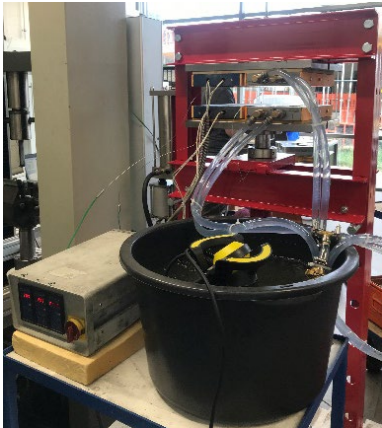


Detailed overview	Image	Description
1. Radiation furnace		<ul style="list-style-type: none"> - Furnace for solution annealing - Solution annealing temperature between 465° and 490°C.
2.1 Plate tool		<ul style="list-style-type: none"> - Plate tool with heating and cooling plates. - Heating plates with four heating cartridges (630watt). - Cooling plates include water cooling channels.
2.2 Forming press		<ul style="list-style-type: none"> - Control device for controlling the heating cartridges (2-Zones). - Water container with water pump for the cooling plates.
3. Temperature logger (sample time 1s)		<ul style="list-style-type: none"> - Temperature data logger to temperature monitoring of the furnace, specimens and tensile testing machine
5. GOM Aramis Adjustable – 2.3M		<ul style="list-style-type: none"> - Deformation and strain measurement - 2.3 MPixel (1936x1216) - 130 frames per second

Table 1: Detailed overview of used testing equipment

2.2 Test procedure

The test procedure can be described as follows:

1. First, the specimens are heated to 465°C in the furnace which takes about 8 minutes. To ensure that all alloying elements are in solution the temperature of the specimen is maintained for 5 minutes.
2. In the next step the samples are transferred within 7 seconds to the plate tool which is preheated to 150°C. The specimens are pressed for 15 seconds applying 5t. This time corresponds to the industrial requirements for a reasonable cycle time which is 15 seconds. This step enables the insertion of a CFRP/GFRP patch which will be bonded by direct thermal joining. At this stage the matrix of the patch acts like an adhesive.
3. Finally, the specimens are tested in a uniaxial tensile testing machine with a climate chamber. The climate chamber is heated up to 150°C to prevent any cooling of the specimen during the test. In addition to the force-displacement measurement an optical measurement of the surface of the specimens is carried out. This is necessary to determine the local equivalent strain at fracture and the anisotropic Lankford-parameters (r-values).

The temperature of the furnace, specimens, heating/cooling plates and climate chamber is monitored throughout the whole process as shown in Figure 3.

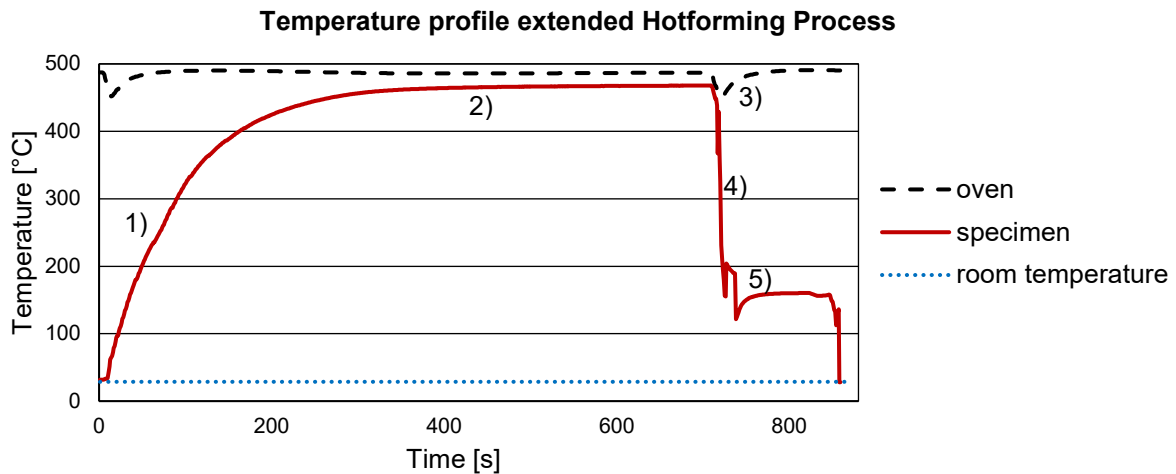


Fig.3: Temperature characteristic of the Extended Hotforming Process

The temperature curve can be divided into the following five areas:

- 1) in the first area the specimens are heated up within 7-8 minutes to 465°C (solution annealing temperature),
- 2) then the specimen is kept at the temperature level of 465°-480°C for 5 minutes,
- 3) transfer from the furnace into the heated plate tool (150°C),
- 4) quenching in the plate tool at approx. 150°C (quenching rate from 400°C to 290°C should be greater than 100°K/s), and
- 5) insertion of the specimens into the tensile testing machine and start testing with optical strain measurement.

From the tensile tests the Lankford parameters, yield stresses (Table 2) and flow curves (Figure 4) were determined from various tensile tests using sheet metal specimens with different rolling directions.

	0°-direction	45°-direction	90°-direction
Lankford-Parameter	$r_0 = 0.44$	$r_{45} = 0.87$	$r_{90} = 0.36$
Yield stress [MPa]	$\sigma_0 = 203$	$\sigma_{45} = 194$	$\sigma_{90} = 204$
Flow curve after Hockett-Sherby	$434 - 203e^{-4.18\varepsilon_p^{0.78}}$	$395 - 194e^{-5.14\varepsilon_p^{0.83}}$	$415 - 204e^{-5.12\varepsilon_p^{0.84}}$

Table 2: Anisotropic parameters

The extrapolation of the flow curves was performed by using the Hockett-Sherby equation [6]. Thereby, the flow curves of the specimens with different rolling directions were approximated and extrapolated as illustrated in Figure 4.

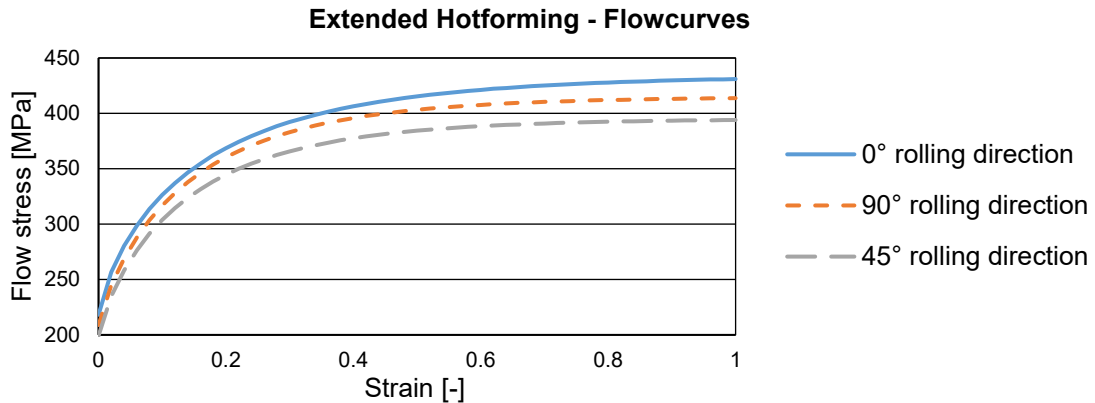


Fig.4: Extrapolated flow-curves after Hockett-Sherby in different rolling directions of the Extended Hotforming Process

2.3 Material model Barlat2000 for Extended Hotforming

The material behaviour during the Extended Hotforming Process can be described with the Barlat YLD2000 [4] material model (LS-Dyna MAT_133) which enables a good illustration of the anisotropy of high strength aluminium alloys. This model requires eight α -values as input variables which are described by the following test values:

- Lankford Parameter: r_0, r_{45}, r_{90}, r_b
- Yield stress: $\sigma_0, \sigma_{45}, \sigma_{90}, \sigma_b$

which are listed in Table 2. The biaxial parameters r_b and σ_b are determined by reverse engineering / parameter optimisation. The aim of the optimisation is to adapt the force-displacement or the stress-strain curves from the simulation to the experimentally determined stress-strain curves. The material model is calibrated with the Software LS-OPT from DYNAmore. The created simulation models of the specimens are illustrated in Table 3.

Tensile test	Notched test	Shear test 0°	Shear test 15°
Shear test 30°	Shear test 45°	Erichsen test	

Table 3: Overview of the simulation models for material and damage/ failure model calibration

In each of these simulation models the eight α -values of the Barlat YLD2000 material model are parametrised. In addition, a *Matlab* script is created for the conversion of the experimental data $(r_0, r_{45}, r_{90}, r_b, \sigma_0, \sigma_{45}, \sigma_{90}, \sigma_b)$ into the Barlat α -values, where σ_b and r_b are used as optimisation parameters.

The procedure of the optimisation can be described as following:

- 1) The input values $r_0, r_{45}, r_{90}, r_b, \sigma_0, \sigma_{45}, \sigma_{90}$ and σ_b are transferred into *Matlab* where the yield strengths are normalised to σ_0 .
- 2) Those input values are used to calculate the eight α -values of the Barlat YLD2000 material model which are implemented to the seven simulation models (as shown in Table 3).
- 3) After successful simulation the stress-strain curves are evaluated. From the Erichsen test the force-displacement characteristics are analysed. For each test the deviation between the predicted curve and the experimentally determined curve is determined. The r_b and σ_b values are optimised by the optimisation software minimising the corresponding deviation value by means of *curve fitting*.

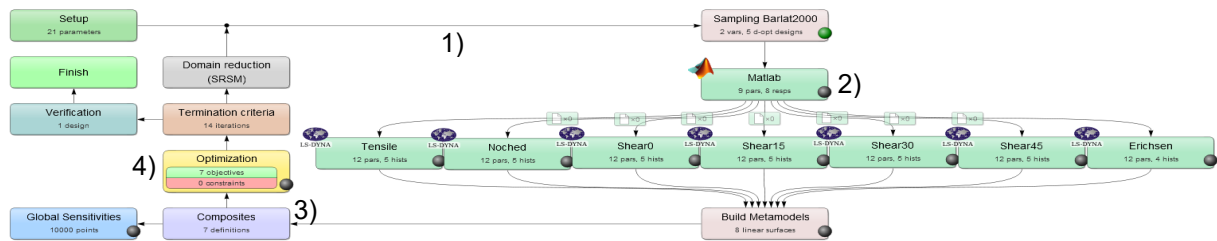


Fig.5: LS-OPT structure of the material and damage/ failure calibration

Table 4 shows the optimised parameters.

α_1	α_2	α_3	α_4	α_5	α_6	α_7	α_8
0.861	1.080	2.292	1.318	0.959	0.656	1.030	0.781

Table 4: Parameters for the calibrated Barlat YLD2000 material model of AA7075 Hotforming material

The optimised stress-strain curves and force-displacement curves are shown in Table 5. The black curves are the experimental data and the green curves are the numerically predicted curves using the Barlat YLD2000 model for the Extended Hotforming Process.

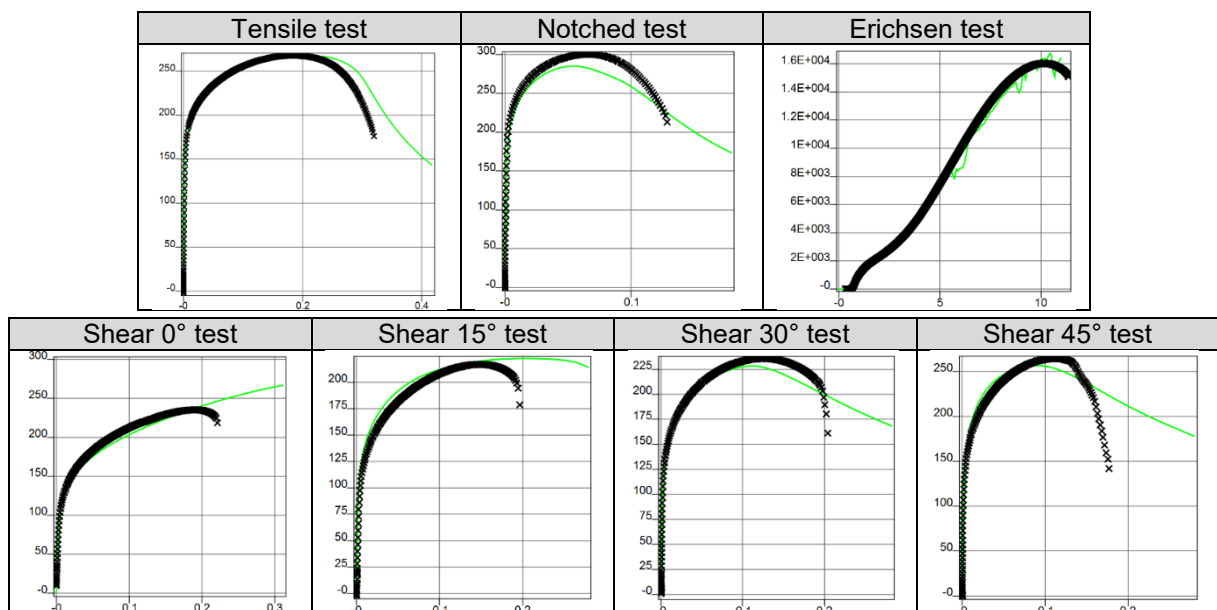


Table 5: Comparison of experimentally and numerically determined stress-strain curves and force-displacement diagrams using Barlat YLD2000 model

2.4 Damage-/ Failure model GISSMO

The calibration of the failure model is carried out in the same manner as the calibration of the material model as shown in Figure 5. For this purpose, the same simulation models, which are illustrated in Table 3, are used. In addition, the damage/ failure model GISSMO is parameterised. For this, the triaxial-failure-curve (TFC) and material-instability-curve, also called E_{crit}, is adjusted according to the existing experimental data. The previously optimised Barlat YLD2000 is used for the material model.

GISSMO is used for the prediction of necking and fracture of the material when exposed to the Extended Hotforming Process. For further crash investigations it is possible to map the plastic strain, thinning and damage to the crash simulation model to be able to reach higher quality of results. To describe the failure and instability curve three distinctive triaxialities are chosen.

- Pure shear stress ($\eta = 0$)
- Pure tensile stress ($\eta = 0.333$)
- Pure biaxial stress ($\eta = 0.666$)

The associated plastic failure and instability strain are parameterised as shown in Table 6.

Triaxiality	Failure strain		Instability strain	
	Parameter (TFC)	Optimised value	Parameter (E _{crit})	Optimised value
0	TR0	1.252	ECR0	0.950
0.111	TR1	0.426	-	-
0.222	TR2	0.502	-	-
0.333	TR3	1.125	ECR3	0.249
0.444	TR4	0.714	-	-
0.555	TR5	0.548	-	-
0.666	TR6	0.855	ECR6	0.855

Table 6: Parameterization and results of the failure and instability curve

The TFC- and E_{crit}-parameters (TR0 to TR6 and ECR0 to ECR6), as shown in Table 6, are varied by the optimisation software until necking and fracture of each specimen corresponds to the experiment as illustrated in Table 7.

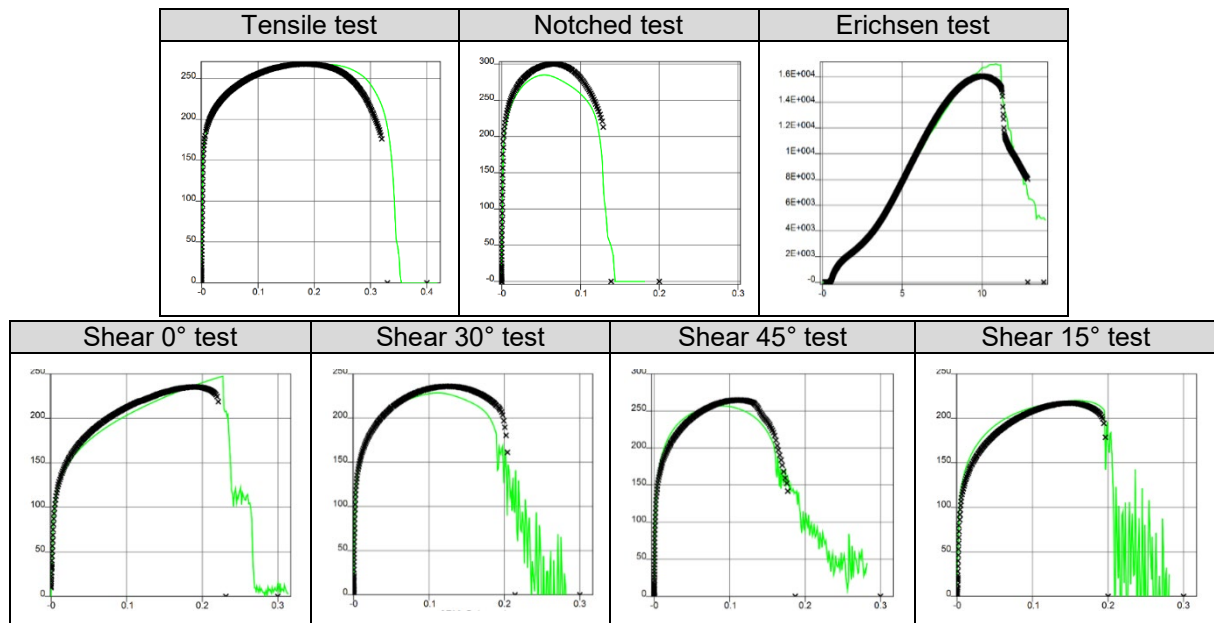


Table 7: Optimization results for damage/ failure model stress-strain and force-displacement diagrams

In Figure 6 the triaxial-failure curve (TFC) and the instability curve (Ecrit) of an AA7075 material applied to the Extended Hotforming Process is shown which are generated using the optimised values listed in Table 6.

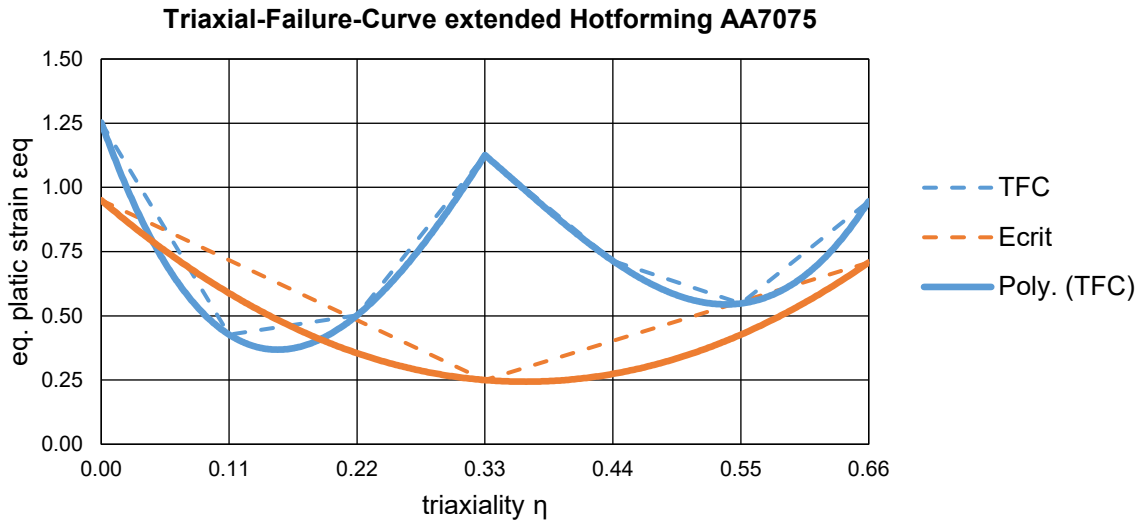


Fig.6: Triaxial failure curve of the Extended Hotforming Process using AA7075 material

3 Conception of a demonstration part

The side impact beam is selected to demonstrate the feasibility of manufacturing in various forming processes at elevated temperatures (Warm- and Hotforming processes). The geometry of the side impact beam is scalable so that the component can be produced using the existing equipment (forming press, dynamic bending and drop testing apparatus).

3.1 Determination of loads and boundary conditions

A side impact beam is of great importance in the event of a side impact in a car accident for example where the vehicle is thrown sideways against rigid objects (e.g. trees). Such accidents often result in serious or fatal injuries. Therefore, passenger cars are subjected to the EURO NCAP pole impact test [7]. Due to the localised load the deformation of the side impact beam can be very high and the counterpart can penetrate deep into the passenger compartment. As shown in Figure 7 the vehicle is driven against a pole at a speed of 32 km/h (8.89 m/s) and at an angle of 15°. The point of impact is at the height of the driver's centre of gravity.



Fig.7: NCAP side impact test [7]

In order to determine the loads and boundary conditions of the side impact beam an existing and freely available simulation model of a Toyota Yaris [8] (Figure 8) is used.

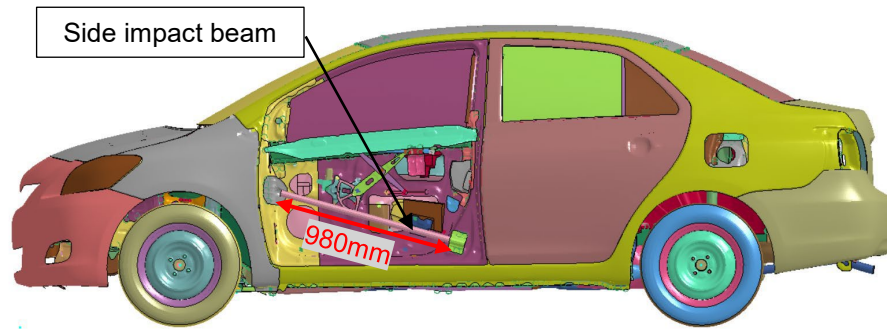


Fig.8: Side impact beam of a Toyota Yaris [8]

Analogue to the EURO NCAP pole impact test a simplified model of a drop test is designed and implemented into the FEM simulation software. After analysing the deformation of the press hardened steel side impact beam, which is set as default in the full Toyota Yaris FE-model, it can be seen the deformation behaviour is equal as shown in a dynamic three-point bending test (Figure 9). The connection points to the door behave like hinges. To minimise the computational time the complexity of the hinge joint is simplified (Figure 9). Thus, the hinge joint (height 50 mm) is defined as a rigid body with one degree of freedom around the y-axis and a distance of 980 mm, which is given by the original Toyota Yaris model. The adapter plate hinge joint and some elements of the side impact beam (uniform shell elements) are fixed together (tied contact). In addition, the initial velocity and mass of the impactor (uniform shell elements), are also defined as a rigid body ($v_0 = \sim 4430 \frac{mm}{s}$ and $m = 40 \text{ kg}$), having the same internal energy as the original full Toyota Yaris side impact beam.

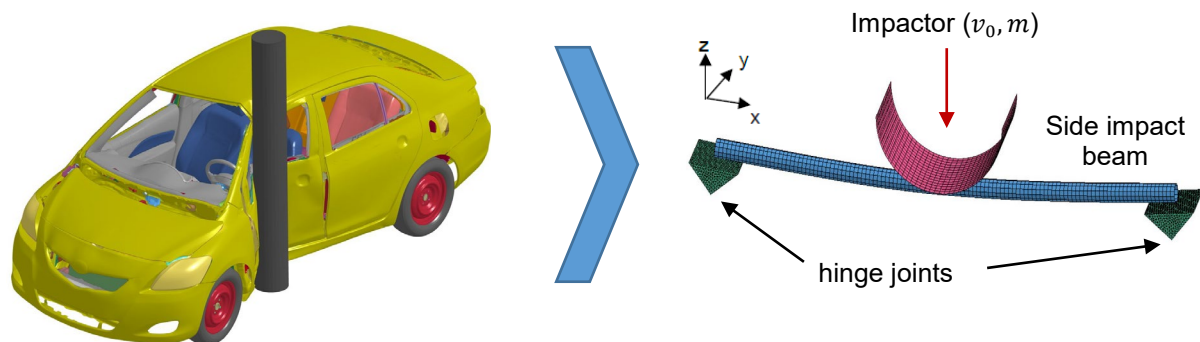


Fig.9: Full Toyota Yaris FE-model - NCAP pole test and simplify FE-Model

3.2 Design guidelines side impact beam

Figure 10 shows the dimensions of the initial side impact beam (press-hardened steel (phs) tube $\varnothing 30 \text{ mm}$). From the design guidelines [8] a minimum distance of the beam from the glass (25 mm) and from the door inner (4mm) is specified. The design space for the new beam is set to the following dimensions:

- Length of 980 mm
- Width 105 mm
- Depth of 30 mm
- Thickness 2.0 mm
- 25 mm distance from the glass
- 4 mm distance from the door inner

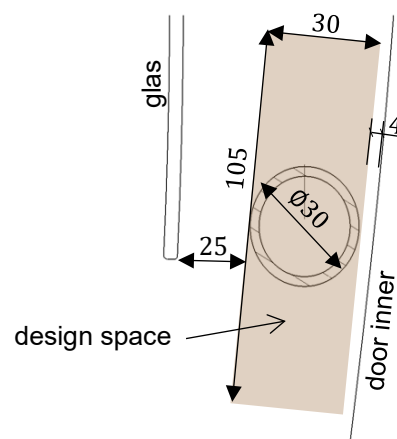


Fig.10: Design space for topology optimisation

4 Topology optimisation

For the determination of a cross section with a high energy absorption, when substituting the press-hardened steel with AA7075 material, a topology optimisation is carried out. The topology optimisation is performed using the static optimisation method [9].

4.1 Optimisation setup

The topology optimisation requires the specification of a design space that describes the maximum possible space (see Figure 10 - brown rectangle) of the component. Figure 11 shows the simulation model with corresponding loads and boundary conditions. In order to reduce the optimisation time a half model with symmetrical boundary conditions is used. The hinge and punch are modelled with shell elements and are defined as rigid bodies. Their support is in their centre of gravity. These are connected to the shell elements with connectors. A mass of 20 kg is applied to the impactor. A

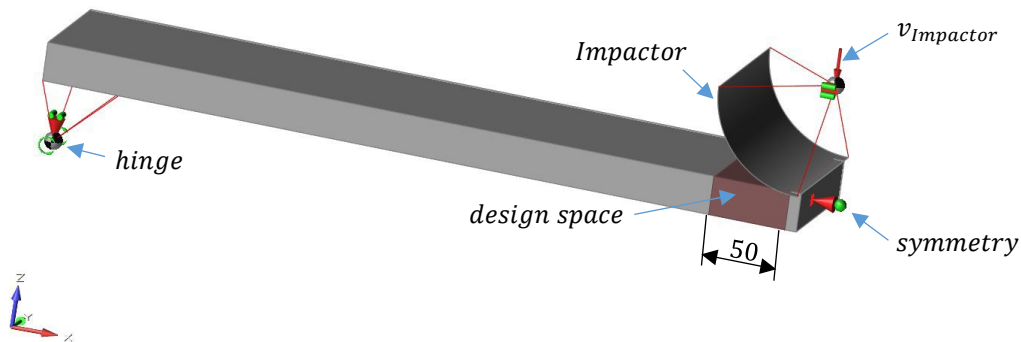


Fig.11: Simulation model for topology optimisation

To find a suitable cross-section and to minimise the computational time a small design space was defined near the impactor where the largest deformation takes place. This also avoids defining boundaries and loads in the design space. As shown in Figure 11 the design space is defined with a length of 50 mm. Due to different forming processes certain design restrictions which are mainly based on practical experience are considered for the beam design.

For this purpose, the following restrictions are incorporated into the optimisation:

- the objective function is to maximise the stiffness of the part and to reduce the mass of the part to 15%,
- Double-sided demoulding (split draw) with the option "no hole" as a production restriction, and
- Minimum material thickness of 2 mm, which corresponds to sheet thickness of the blank.

4.2 Optimisation results

The result of the static topology optimisation is shown in Figure 12. It shows that the predicted cross-section corresponds to a W-profile (Figure 12 b).

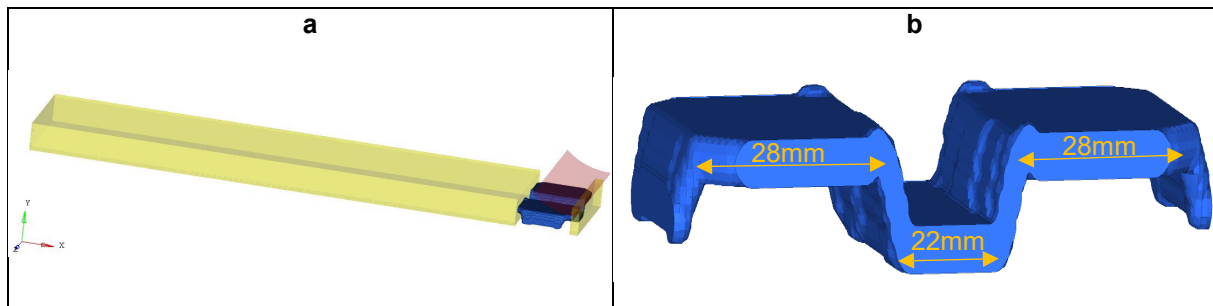


Fig.12: Result of the topology optimisation

5 Design of a demonstration part

Based on the topology optimisation and the design guidelines a new lightweight side impact beam made out of AA7075 is designed. For further considerations it is not necessary to produce the full length of the side impact beam. Therefore, the length of the beam is set to 300 mm. The newly designed side impact beam is shown in Figure 13.

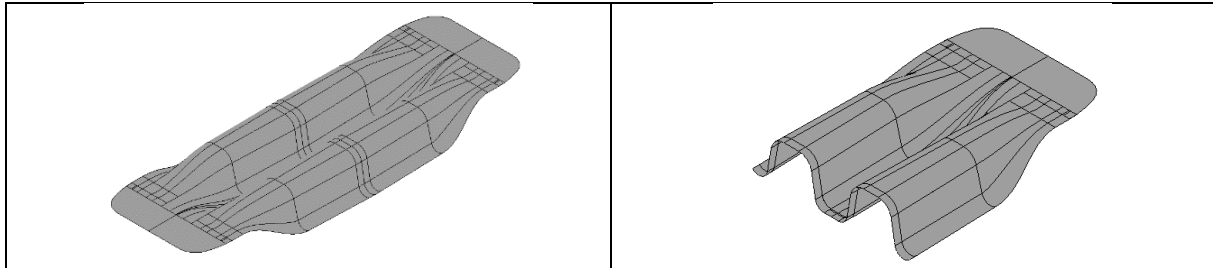


Fig. 13: Functional model of the side impact beam

6 Summary

A novel process, named “Extended Hotforming Process” which is based on the common Hotforming process and the “Thermal Direct Joining Process” is investigated. For an accurate prediction of the material behaviour when applied to the Extended Hotforming Process it is important to determine the accurate material and failure models. Thus, the Barlat YLD2000 material model and the GISSMO damage- and failure model are used which consider anisotropy effects of rolled high strength aluminium material and any necking or cracking mechanisms. For an adequate characterisation of those models experimental tests with various specimen geometries (tension, shear, notched and Erichsen test), applying different stress conditions ($-1/3 < \eta < 2/3$), are carried out. Further, for the determination of the stress-strain curves and the local strains at fracture an adapted optical measurement system is used. Subsequently, parameter optimisations using LS-OPT are carried out to optimise and fit the alpha values required for the Barlat YLD2000 material model, the Triaxial-Failure curve and the instability curve for the GISSMO damage and failure model. The predicted stress-strain data show good correlation with the experimental results for all loading states (shear, tensile, notched and biaxial).

Based on the Euro NCAP pole test boundary and load cases are derived and adapted to a dynamic 3-point bending test. Subsequently, a topology optimisation is carried out to find a good design for a sheet metal side impact beam and to replace the present side impact tube made out of pbs-material. To ensure the formability of the component various manufacturing restrictions are set for the topology optimisation study. As a result it can be seen that the most suitable cross section for a crash relevant component manufactured by the “Extended Hotforming Process” is given by a W-profile. Further investigations will be carried out based on this study.

7 Literature

- [1] e-mobil BW GmbH – Landesagentur für Elektromobilität und Brennstoffzellentechnologie Baden- Württemberg, Ministerium für Finanzen und Wirtschaft Baden-Württemberg, Ministerium für Wissenschaft, Forschung und Kunst Baden-Württemberg (2012): Leichtbau in Mobilität und Fertigung, 2012
- [2] Schlosser, J.: “Characterisation and optimisation of a failure-model for high strength aluminium alloys”, *Advances in manufacturing technology XXXII*, 16 (2018), pp.399-404
- [3] Impression Technologies Limited, “Method of forming components from sheet material”, 2006, WO2017/093767
- [4] Barlat, F.: “Plane stress yield function for aluminum alloy sheets – part 1: theory”, *Int. J. Plasticity*, 19 (2003), pp. 1297-1319
- [5] Barlat, F.: “Plastic behavior and stretchability of sheet metals. Part I: A yield function for orthotropic sheets under plane stress conditions”, *Int. J. Plast.*, 5 (1989), pp. 51-66
- [6] Hockett, J.E.: “Large strain deformation of polycrystalline metals at low homologous temperatures”, *J. Mech. Phys. Solids*, 23-2 (1975), pp. 87-98
- [7] Euro NCAP; accessed 19 January 2019, <https://www.euroncap.com/de/fahrzeugsicherheit/die-bedeutung-der-bewertungen/insassenschutz-fuer-erwachsene/pfahlaufpralltest/>
- [8] National Highway Traffic Safety Administration, accessed 20 June 2018, <https://www.nhtsa.gov/crash-simulation-vehicle-models>
- [9] Altair HyperWorks, “Altair OptiStruct User Guide”, 2017, pp. 539-557